Analysis of a High Resolution Planar PKM

Olivier Company, Sébastien Krut, François Pierrot

Analysis of a High Resolution Planar PKM

Olivier Company, Sébastien Krut, François Pierrot
LIRMM, Univ. Montpellier 2, CNRS
161 rue Ada, 34392 Montpellier, France

Abstract — **This paper presents a kinetostatic analysis of a planar parallel mechanism intended to be used in high accuracy operation. The machine architecture is peculiar in at least two aspects: it is designed to operate in a near-singularity configuration and is build with flexible joints. Kinematic and kinetostatic modeling allow to evaluate the theoretical improvement of the resolution, as well as forces created by both inertial effects and elastic deformation of joints. The final design of the micro-stage is presented as well as the obtained prototype.**

I. Introduction

Positioning problems are becoming crucial in many industries such as microelectronics. At the present time, research issues concern accuracy, repeatability, resolution and speed for precision positioning mechanisms. We propose to address this important issue with a novel macro/micro machine architecture composed of two stages: a macro-stage for coarse motion presented by authors [1] and a micro-stage for fine motion. We focus in this paper on the micro-stage that will achieve the high resolution and fast positioning; it combines three features: planar parallel mechanism, near singular configuration, flexible joints.

The choices for such a combination of features have been detailed in [2]. We will focus in this paper on the flexible joints, and more precisely on the force modeling. Concerning flexible links, several bibliographic papers were written to model their behavior. We can cite two major books written by Howell [3] and Henein [4] that try to cover the complete range of flexible links, as well as some modeling methods for multiple instances of flexible links in assemblies and examples on realized prototypes. Another interesting approach has been more focused on flexible links realized by machining down of material on a part: circular notch flexure hinge [5]. Criteria for the choice of the link material, the behavior of elastic beams and their use to realize flexible links are detailed. Two prototypes of spatial parallel manipulators have been presented by Harai *et al* [6] and Chung *et al* [7]. The first one possesses 3-DOF (Degrees Of Freedom) in translation along the three axis of space. The second one also possesses 3-DOF, but they are 1T-2R (T stands for translation and R for rotation). Both mechanisms contain monolithic (composed of one unique part) kinematic chains made of flexible links. To get closer from what we want to work on, two studies written by Hesselbach *et al* [8] and Yi *et al* [9] concern planar parallel structures utilizing flexible links. The first one proposes a modeling of flexible notch hinge and then includes it into a planar parallel mechanism. The second one investigates a planar parallel flexible links mechanism with two different kinds of flexible links: one composed of 1-DOF (1R) flexible links, and one composed of 2-DOF (1T-1R) flexible links. The stiffness model is investigated for both kinds of flexible links. Finally, a force-torque sensor has been developed using a spatial parallel mechanism in a near singular configuration using flexure hinges by Ranganath [10]. This concept has been used to build a prototype based on the Gough platform. Some experimental results showed the sensitivity of the structure relatively to the externally applied forces and moments.

II. General architecture of the micro-stage

As mentioned above, the global architecture of the machine is a 3-axis, planar "macro/micro" mechanism: a macro-stage for coarse motion and a micro-stage for fine motion. The macro-stage has been previously studied in [1] and in this paper, we focused on the micro-stage. Due to the resolution of positioning expected for the macro-stage (a few microns), we chose for the workspace of the micro-stage a disc of diameter ∅0.2 mm with an orientation of ±0.1 °. This could seem a lot larger than the positioning resolution of the macro-stage, but the reason of this choice was mainly to overcome potential errors in modeling, manufacturing, assembly and experimental process measurements that could occur.

The micro-stage will be realized with a parallel structure. Indeed, parallel architecture offers many advantages well suited to this application (see [11] for an overview of this topic), among which we can cite:

- The separation of the actuation (fixed on the base and producing thermal effects) from the traveling plate
- Light weight moving parts: the actuators are fixed on the base, so the traveling plate does not have to support the weight of the actuators.
- The stiffness of the mechanism is improved compared to serial architectures.

Another interesting feature of parallel mechanisms are their singular configurations. A classification has been proposed by Zlatanov *et al [12]*, distinguishing parallel, serial and internal singularities (serial, parallel and constraint singularities). We focused here on *serial singularity*, because in their neighborhood, the positioning resolution of the ending part is improved. Indeed, for a small movement of the actuator, the resulting movement of the traveling plate is smaller hence the reduction ratio is improved without any additional mechanical element.

Another interesting aspect of the micro-stage concerns the fact that all the links are realized using flexible links, which avoid the drawbacks of conventional links: wear, backlash, friction, stick-slip effect… These drawbacks are often the main source of errors when trying to create precise positioning mechanisms [13].

To summarize the overall architecture, the micro-stage will be composed of a planar **parallel** mechanism in a **near serial-singular configuration**. Moreover, all the **joints** will be made **flexible**.

III. 3 RRR micro-stage with PRR actuation

The micro-stage has to achieve a planar motion, that is to say 3-DOF: two translations along the x and y axis and one rotation around the z axis. This motion will be parameterized by three parameters (x, y, θ).

Different kinds of planar parallel mechanisms composed of P and R joints exist (assumption: a planar parallel mechanism is composed of three kinematic chains), being combinations of three of the seven possible planar chains: RPR, RRR, PRR, RPP, PRP, PPR, RRP. These planar mechanisms have been investigated by Merlet [14]. Fig. 1 represents a general class of planar parallel manipulators. Points A_i, B_i, C_i ($i = 1,..., 3$ stands for the number of the kinematic chain) represent the centers of the joints that are P or R. D represents the center of the traveling plate. A coordinate system is attached to the traveling plate: $R_t(D, x_t, y_t, z)$; another one is attached to the frame: $R_b(O, x_b, y_b, z)$. The angle θ represents the orientation of the traveling plate relatively to the frame.

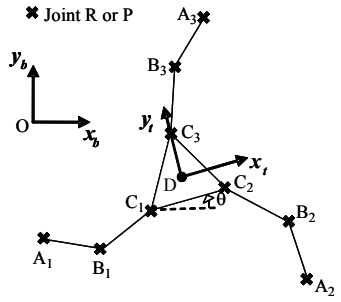

Fig. 1 General class of planar parallel manipulators

A complete kinematic analysis of all these planar parallel mechanisms has been conducted by Williams *et al* [15], as well as their direct kinematics that has been investigated by Merlet [16].

The first point we focused on is the arrangement of joints for one kinematic chain, then for the complete mechanism. After a study of the different possibilities to realize flexible joints (see [3] and [4]), we decided to consider only revolute joints, and to realize the flexible links as flexible circular notch hinge. Indeed, these joints are easy to manufacture (less parts than prismatic flexible joints), and they are well adapted to kinematic structures composed of multiple instances of flexible links. This directly led to a RRR arrangement for a chain of the planar parallel mechanism. Then, for symmetry consideration, the mechanism is realized with three identical RRR chains. The symmetrical aspect of the mechanism (120 ° symmetry) ensured that potential errors on the geometry would have symmetrical consequences on the final result.

The second point we focused on was the way the actuation is realized. It was preferable not to actuate the mechanism thanks to a revolute actuator, because this would have resulted into bending of parts. This is why we decided to use an additional PRR mechanism (see Fig. 2), composed of a rod connected with two more flexible revolute joints to a prismatic linear actuator on one side and to the RRR chain on the other side. This mechanism offers the possibility to avoid the bending of parts. This solution also ensured that any potential error on the straightness of the actuator guide-way would have no direct consequences on the final resolution of positioning of the mechanism.

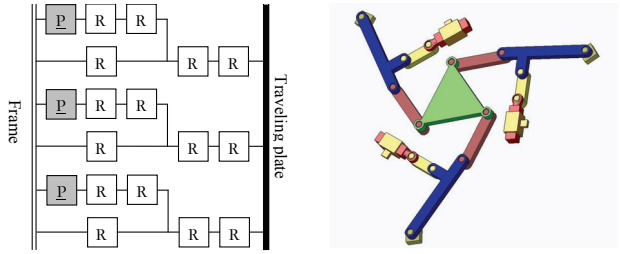

Fig. 2 Schematic view of the micro-stage

IV. Kinematic modeling

The geometry chosen to represent one kinematic chain of the micro-stage is detailed in Fig. 3 and Fig. 4 represents the same kinematic chain, once manufactured.

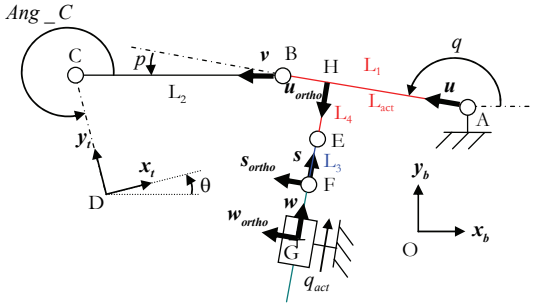

Fig. 3 Notations used in the different modelings

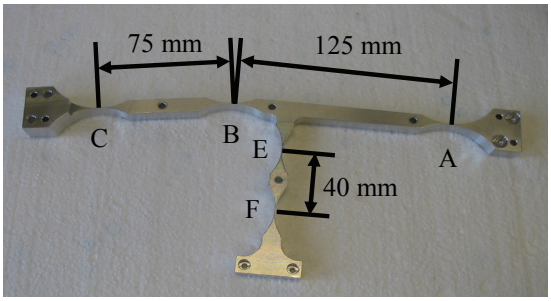

Fig. 4 Flexible machined kinematic chain

- u, v, w, s, u_{ortho} respectively represents the unitary vectors of parts going from A to B, B to C, G to F, F to E, and H to E. w_{ortho} and s_{ortho} respectively represents the unitary vectors orthogonal to w and s.
- G is the origin of the actuator. Points A and G are attached to the frame. D is the center of the traveling plate (moving element).
- L_1, L_2, L_3, L_4 and L_{act} are respectively the lengths of segments going from A to B, B to C, E to F, H to E and A to H.

The inverse velocity kinematics solutions give the actuators velocity parameter $\dot{q}_{acti}$ for a given of velocity $(\dot{x}, \dot{y}, \dot{\theta})$ of point D. The whole micro-stage is considered as built with two sub-mechanisms. One is composed of the planar parallel 3-RRR mechanism represented in Fig. 5 by

letters $A_iB_iC_iD_i$ ($i = 1, 2, 3$, represents the number of the studied kinematic chain), and the second one is the decoupled actuating PRR mechanism represented in Fig. 5 by the letters $A_iE_iF_iG_i$.

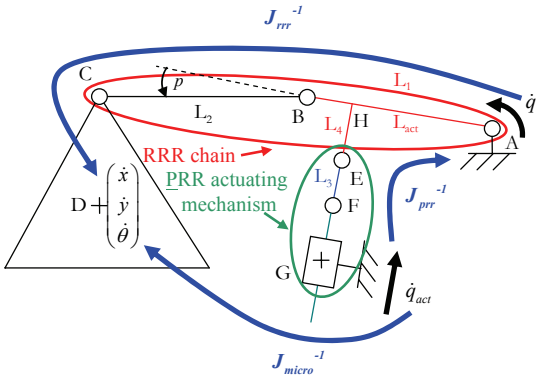

Fig. 5 Sub-mechanism and matrix decomposition

The velocity relationship is obtained as follows (see [2] for a complete and detailed modeling):

$$\dot{\boldsymbol{q}}_{act} = \boldsymbol{J}^{-1}\dot{\boldsymbol{x}} \tag{1}$$

with $\dot{\boldsymbol{q}}_{act} = \begin{pmatrix} \dot{q}_{act1} \\ \dot{q}_{act2} \\ \dot{q}_{act3} \end{pmatrix}$, $\dot{\boldsymbol{x}} = \begin{pmatrix} \dot{x} \\ \dot{y} \\ \dot{\theta} \end{pmatrix}$,

and $$\boldsymbol{J}^{-1} = \boldsymbol{J}_{prr}^{-1}\boldsymbol{J}_{rrr}^{-1} \tag{2}$$

where $\boldsymbol{J}_{rrr}^{-1} = \boldsymbol{J}_{q\,rrr}^{-1}\boldsymbol{J}_{x\,rrr}$ and $\boldsymbol{J}_{prr}^{-1} = \boldsymbol{J}_{q\,act}^{-1}\boldsymbol{J}_{q\,prr}$.

The four matrices $\boldsymbol{J}_{q\,rrr}$, $\boldsymbol{J}_{x\,rrr}$, $\boldsymbol{J}_{q\,act}$ and $\boldsymbol{J}_{q\,prr}$ are defined as follows:

$$\boldsymbol{J}_{q\,rrr} = \begin{pmatrix} \boldsymbol{v}_1 \bullet \boldsymbol{u}_{ortho\,1} & 0 & 0 \\ 0 & \boldsymbol{v}_2 \bullet \boldsymbol{u}_{ortho\,2} & 0 \\ 0 & 0 & \boldsymbol{v}_3 \bullet \boldsymbol{u}_{ortho\,3} \end{pmatrix}$$

$$\boldsymbol{J}_{x\,rrr} = \begin{pmatrix} v_{x1} & v_{y1} & (\boldsymbol{C}_1\boldsymbol{D} \times \boldsymbol{v}_1)_z \\ v_{x2} & v_{y2} & (\boldsymbol{C}_2\boldsymbol{D} \times \boldsymbol{v}_2)_z \\ v_{x3} & v_{y3} & (\boldsymbol{C}_3\boldsymbol{D} \times \boldsymbol{v}_3)_z \end{pmatrix}$$

$$\boldsymbol{J}_{q\,act} = \begin{pmatrix} (\boldsymbol{w}_1 \bullet \boldsymbol{s}_1) & 0 & 0 \\ 0 & (\boldsymbol{w}_2 \bullet \boldsymbol{s}_2) & 0 \\ 0 & 0 & (\boldsymbol{w}_3 \bullet \boldsymbol{s}_3) \end{pmatrix}$$

$$\boldsymbol{J}_{q\,prr} = \begin{pmatrix} (L_{act}\boldsymbol{u}_{ortho1} - L_4\boldsymbol{u}_1) \bullet \boldsymbol{s}_1 & 0 & 0 \\ 0 & (L_{act}\boldsymbol{u}_{ortho2} - L_4\boldsymbol{u}_2) \bullet \boldsymbol{s}_2 & 0 \\ 0 & 0 & (L_{act}\boldsymbol{u}_{ortho3} - L_4\boldsymbol{u}_3) \bullet \boldsymbol{s}_3 \end{pmatrix}$$

{ Note: • represents the dot product, and × represents the cross product.}

V. Flexible link modeling and forces evaluation

In this section, we will introduce the flexible circular notch hinge, detail its characteristics, and present a modeling of the efforts generated by such a link.

Flexible circular notch hinge

After a study of the different possibilities to realize flexible joints ([3] and [4]), we decided to model all the flexible joints as revolute joints R, and to realize these flexible links as flexible circular notch hinge (see Fig. 6). Indeed, these joints are easy to study and to manufacture (much less parts than prismatic flexible joints), and they are well adapted to multiple instances of flexible links.

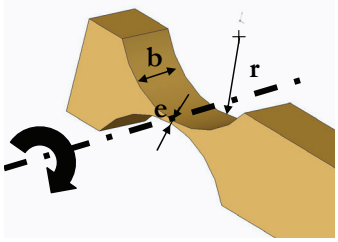

Fig. 6 Parameterization of a flexible circular notch hinge

The two main characteristics of such a link stand in its angular stiffness K_α and its angular stroke α (defined by (3)), both depending on the material and on the geometrical properties of the link: e, b, r.

$$K_\alpha = \frac{2Ebe^{2,5}}{9\pi\sqrt{r}} \text{ and } \alpha = \frac{3\pi\sigma_{adm}\sqrt{r}}{4E\sqrt{e}} \tag{3}$$

The dimensions chosen for the flexible links are $e = 0.5$ mm, $r = 30$ mm and $b = 10$ mm (these dimensions are consistent with the recommendations for standard flexible circular notch hinge described by Henein [4]). The chosen material is Alu7075 (high elastic limit aluminum alloy), with $E = 72{,}000$ MPa and $\sigma_{adm} = 500$ MPa. Thus, we obtain the following characteristics for the flexible links:

$$K_\alpha = 1.64 \text{ N.m/rad and } \alpha = 7.26 \text{ deg} \tag{4}$$

The value of α allows us to verify and validate the choice of this type of flexible link. Indeed, it is very important to verify that the angular strokes of the revolute joints R for the whole micro-stage obtained thanks to the inverse kinematics are smaller than α. Simulations have shown that the maximum angular stroke at point B (angle p) is 4deg, thus smaller than 7.26deg. The obtained angular stiffness K_α will be used in the modeling and evaluation of forces generated by the flexible links.

Modeling of the forces of the micro-stage

The major forces acting on the micro-stage come from two different sources: inertial forces due to the traveling plate motion, and flexible links inside the mechanism.

1) Inertial forces

External forces exerted on the traveling plate can be mapped onto actuator forces thanks to the force/velocity duality property:

$$\boldsymbol{F}_{act\,ext} = \boldsymbol{J}^T\boldsymbol{F}_{ext} \tag{5}$$

$\boldsymbol{J}$ has been defined in (2); $\boldsymbol{F}_{act\,ext}$ represents the vector of actuator, its dimension is 3×1; $\boldsymbol{F}_{ext}$ represents the vector of external forces applied on the micro-stage and expressed at the center of the traveling plate D, its dimension is 3×1: it is supposed here to represent only inertial forces. These two vectors are defined as follows:

$$\boldsymbol{F}_{act\,ext} = \begin{pmatrix} F_{act\,ext1} \\ F_{act\,ext2} \\ F_{act\,ext3} \end{pmatrix} \text{ and } \boldsymbol{F}_{ext} = \begin{pmatrix} m\,a_x \\ m\,a_y \\ J_z\,\gamma_z \end{pmatrix}$$

Where m represents the mass of the micro-stage, a_x and a_y relatively represents the $\boldsymbol{x}$ and $\boldsymbol{y}$ components of the linear acceleration vector $\boldsymbol{a}$. γ_z represents the angular acceleration and J_z represents the inertia around the z axis.

2) Forces due to flexible links

In the modeling of forces, flexible circular notch hinge can be considered as torsional springs, and then the efforts in flexible links can be modeled as a pure torque:

$$\boldsymbol{\Delta C_{flex} = K \Delta \theta} \tag{6}$$

where $\boldsymbol{\Delta C_{flex}}$ represents the vector of torque generated at each flexible link; its dimension is 15×1. $\boldsymbol{K}$ represents the stiffness matrix composed of the stiffness of each flexible link on its diagonal elements; its dimension is 15×15. And $\boldsymbol{\Delta \theta}$ represents the vector of angular variation at each flexible link; its dimension is 15×1.

It is also possible to express the angular variation at each link as a function of the variation of position of point D thanks to matrix $\boldsymbol{M}^{-1}$:

$$\boldsymbol{\Delta \theta = M^{-1} \Delta x} \tag{7}$$

where $\boldsymbol{\Delta x}$ is the vector representing the variation of position of point D, its dimension is 3×1 and it is defined as follow:

$$\boldsymbol{\Delta x} = \begin{pmatrix} \Delta x \\ \Delta y \\ \Delta \theta \end{pmatrix}$$

The matrix $\boldsymbol{M}^{-1}$ will be defined later in V.3), its dimension is 15×3. Thanks to the force/velocity duality property, (7) is equivalent to:

$$\boldsymbol{\Delta F_{flex} = \left(M^{-1} \right)^T \Delta C_{flex}} \tag{8}$$

where $\boldsymbol{\Delta F_{flex}}$ is the vector representing the efforts generated by the flexible links, and expressed at the centre of the travelling plate D, its dimension is 3×1. $\boldsymbol{\Delta F_{flex}}$ can be expressed as follows:

$$\boldsymbol{\Delta F_{flex}} = \begin{pmatrix} \Delta F_{flex\ x} \\ \Delta F_{flex\ y} \\ \Delta C_{flex\ z} \end{pmatrix}$$

Combining (6), (7) and (8), we finally obtain an evaluation of the forces due to flexible links, expressed at point D.

$$\boldsymbol{\Delta F_{flex} = \left(M^{-1} \right)^T K M^{-1} \Delta x} \tag{9}$$

Then, is it possible to map these forces in the actuated-joint space as follows:

$$\boldsymbol{F_{act\ flex} = J^T F_{flex}} \tag{10}$$

where $\boldsymbol{F_{act\ flex}}$ represents the vector of forces generated by the flexible links and expressed at the actuator origin G, its dimension is 3×1. $\boldsymbol{F_{act\ flex}}$ is defined as follows:

$$\boldsymbol{F_{act\ flex}} = \begin{pmatrix} F_{act\ flex1} \\ F_{act\ flex2} \\ F_{act\ flex3} \end{pmatrix}$$

3) Expression of matrix $\boldsymbol{M^{-1}}$

To express matrix $\boldsymbol{M^{-1}}$, we will separate the micro-stage into two sub-mechanisms, as we did for kinematics modeling.

a) Planar parallel 3-RRR mechanism $A_iB_iC_iD_i$

We can express the velocities at points A_i, B_i, and C_i as functions of the velocity of point D. We obtain the following relation for the kinematic chain i:

$$\boldsymbol{\dot{q}_{chi} = J_{chi}^{-1} \dot{x}} \tag{11}$$

with $\boldsymbol{\dot{q}_{chi}} = \begin{pmatrix} \dot{\theta}_{Ai} \\ \dot{\theta}_{Bi} \\ \dot{\theta}_{Ci} \end{pmatrix}$ and $\boldsymbol{\dot{x}} = \begin{pmatrix} \dot{x} \\ \dot{y} \\ \dot{\theta} \end{pmatrix}$

and $$\boldsymbol{J_{chi}^{-1} = \left(J_{qi} \right)^{-1} J_{xi}} \tag{12}$$

where $\boldsymbol{\dot{q}_{chi}}$ represents the vector of velocity of one chain of the planar parallel 3-RRR mechanism, that is to say the velocities at points A_i, B_i and C_i, its dimension is 3×1. The matrices $\boldsymbol{J_{qi}}$ and $\boldsymbol{J_{xi}}$ are defined as follows:

$$\boldsymbol{J_{qi}} = \begin{pmatrix} \left(\left(l_1 \boldsymbol{u_{orthoi}} + l_2 \boldsymbol{v_{orthoi}} \right) \bullet \boldsymbol{x} \right) & \left(l_2 \boldsymbol{v_{orthoi}} \bullet \boldsymbol{x} \right) & 0 \\ \left(\left(l_1 \boldsymbol{u_{orthoi}} + l_2 \boldsymbol{v_{orthoi}} \right) \bullet \boldsymbol{y} \right) & \left(l_2 \boldsymbol{v_{orthoi}} \bullet \boldsymbol{y} \right) & 0 \\ 1 & 1 & 1 \end{pmatrix}$$

and $$\boldsymbol{J_{xi}} = \begin{pmatrix} 1 & 0 & \left(\boldsymbol{E_i C_i} \bullet \boldsymbol{y} \right) \\ 0 & 1 & -\left(\boldsymbol{E_i C_i} \bullet x \right) \\ 0 & 0 & 0 \end{pmatrix}$$

Note that the dimension of $\boldsymbol{J_{chi}^{-1}}$ is 3×3.

b) Decoupled actuating PRR mechanism $A_iE_iF_iG_i$

Expressing velocity of point E_i leads to the following relations:

$$\begin{pmatrix} \dot{\theta}_{Ei} \\ \dot{\theta}_{Fi} \end{pmatrix} = \boldsymbol{J_{rodi}} \dot{\theta}_{Ai} \tag{13}$$

and $$\boldsymbol{J_{rodi} = J_{ai}^{-1} J_{bi}} \tag{14}$$

where matrices $\boldsymbol{J_{ai}}$ and $\boldsymbol{J_{bi}}$ are defined as follows:

$$\boldsymbol{J_{ai}} = \begin{pmatrix} 1 & 1 \\ 0 & \left(\left(\boldsymbol{E_i F_i} \times \boldsymbol{z} \right) \bullet \boldsymbol{w_{orthoi}} \right) \end{pmatrix}$$

and $$\boldsymbol{J_{bi}} = \begin{pmatrix} \left(l_1 \boldsymbol{u_{iortho}} - l_4 \boldsymbol{u_i} \right) \bullet \boldsymbol{w_{orthoi}} \\ 1 \end{pmatrix}$$

With (11), we know how to express the velocity at point A_i as a function of point D. Indeed, if we call $\boldsymbol{L_{j\,chi}}$ ($j = 1, 2, 3$) the vector representing the j^{th} line of matrix $\boldsymbol{J_{chi}}$, we obtain the following relation:

$$\dot{\theta}_{Ai} = \boldsymbol{L_{1\,chi}} \boldsymbol{\dot{x}} \tag{15}$$

Hence, we can merge (13) and (15) to obtain:

$$\begin{pmatrix} \dot{\theta}_{Ei} \\ \dot{\theta}_{Fi} \end{pmatrix} = \boldsymbol{J}_{rodi}\boldsymbol{L}_{1\,chi}\dot{\boldsymbol{x}} \qquad (16)$$

c) Complete micro-stage mechanism

We can merge the results found in (11) and (16) and obtain the following relation:

$$\begin{pmatrix} \dot{\theta}_{Ai} \\ \dot{\theta}_{Bi} \\ \dot{\theta}_{Ci} \\ \dot{\theta}_{Ei} \\ \dot{\theta}_{Fi} \end{pmatrix} = \begin{pmatrix} \boldsymbol{J}_{chi}^{-1} \\ \boldsymbol{J}_{rodi}\boldsymbol{L}_{1\,chi} \end{pmatrix} \begin{pmatrix} \dot{x} \\ \dot{y} \\ \dot{\theta} \end{pmatrix} \qquad (17)$$

This gives the expression of matrix $\boldsymbol{M}_i^{-1}$ for one kinematic chain i, as follows:

$$\boldsymbol{M}_i^{-1} = \begin{pmatrix} \boldsymbol{J}_{chi}^{-1} \\ \boldsymbol{J}_{rodi}\boldsymbol{L}_{1\,chi} \end{pmatrix}$$

Finally, for the complete micro-stage (3 kinematic chains), we obtain the following matrix $\boldsymbol{M}^{-1}$ as follows:

$$\boldsymbol{M}^{-1} = \begin{pmatrix} \boldsymbol{J}_{ch1}^{-1} \\ \boldsymbol{J}_{rod1}\boldsymbol{L}_{1\,chi} \\ \boldsymbol{J}_{ch2}^{-1} \\ \boldsymbol{J}_{rod2}\boldsymbol{L}_{1\,chi} \\ \boldsymbol{J}_{ch2}^{-1} \\ \boldsymbol{J}_{rod3}\boldsymbol{L}_{1\,chi} \end{pmatrix}$$

The obtaining of matrices $\boldsymbol{J}_{chi}^{-1}$ et $\boldsymbol{J}_{rodi}$ is detailed in (12) and (14).

Finally, combining (5) and (10), the total force at the actuators is given by:

$$\boldsymbol{F}_{act\ total} = \boldsymbol{F}_{act\ ext} + \boldsymbol{F}_{act\ flex} \qquad (18)$$

B. Simulations and results

We run some simulations using Matlab®. In these simulations, the point of interest of the traveling plate D covers the complete workspace, that is to say a disc of diameter ∅0.2 mm with an orientation of ± 0.1 °.

The linear acceleration is 0.5 m.s^{-2}. The angular acceleration is set here to zero. The maximum force obtained after simulations is $F_{act\ ext} = 4.04$ N.

With the stiffness we calculated before (the same angular stiffness value $K_\alpha = 1,64$ N.m/rad holds for each flexible link of the micro-stage), the maximum force generated by the flexible links is $F_{act\ flex} = 0.0034$ N. It is interesting to note that the actuator force due to flexible links represent about 0.1% of the actuator force due to inertial forces. These forces can be neglected in the control of the machine compared to the external ones.

The total actuator force (see (18)) is about $F_{act\ total} = 4.05$ N. The actuators have been selected thanks to the time cycle we expect (less than 0.5 s) and the forces that are required to be generated. We choose some micro-actuators that have a stroke of 2 mm and that can push up to 7 N (see Fig. 7).

The actuators encoders have a resolution of 0.1 µm, and thanks to the geometry we used (near singular configuration), simulation has shown that the machine is able to offer a (theoretical) resolution of about 16 nm.

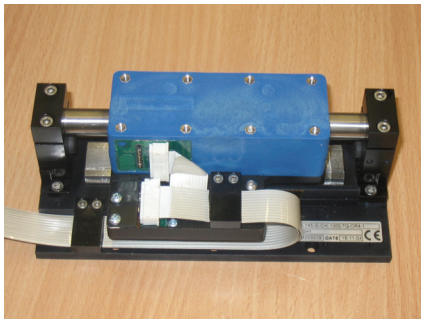

Fig. 7 Chosen micro-actuator

VI. Practical Design of the micro-stage

The micro-stage has been designed with SolidWorks 2004® and then manufactured and assembled. Fig. 8 represents a CAD top view of the micro-stage. We can see on this view the representation of one kinematic chain of the micro-stage as it has been presented in Fig. 3.

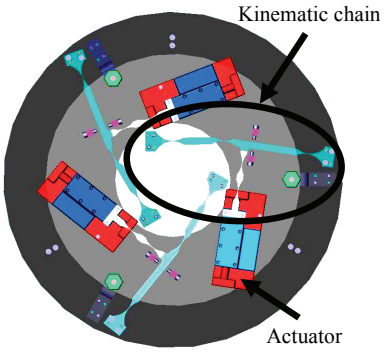

Fig. 8 Top CAD view of the micro-stage

Fig. 9 represents another 3D CAD view of the mechanism. In this picture, we can observe that some mechanical limit stops have been integrated to the final design of the micro-stage. The function of these mechanical limit stops is to avoid any possible deterioration of the flexible links due to a too large displacement.

The supporting system is designed to support the traveling plate in three points, so that the flexible links (RRR and PRR) only work in a rotational motion around an axis normal to the in plane motion. The support of the traveling plate is ensured by 3 flexible hinge, spherical-spherical, chains (see Fig. 11) so that in fact the traveling plate is (at a first order approximation) guided by a equivalent planar joint. Indeed, the exact motion admissible by such a supporting system is a circular translation is circular and an helical rotation. But as the workspace of the traveling space is very small (disc of diameter ∅0,2 mm with an orientation of ±0,1°), the vertical translation generated by these two motions should remain insignificant.

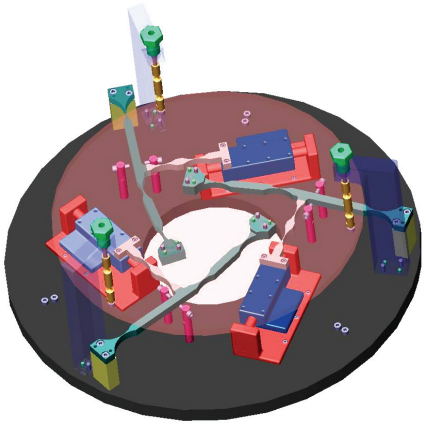

Fig. 9 3D CAD view of the micro-stage

Fig. 10. represents the complete micro-stage mounted on the macro-stage.

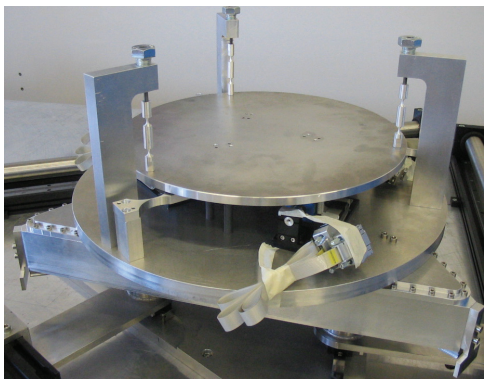

Fig. 10 Complete micro-stage with three supporting legs.

The spherical-spherical link has been designed by removing material on a spherical shape to let a thickness of 2 mm. The forces necessary to move this support mechanism that is also flexible have been estimated using finite element analysis (another possibility of modeling would have been to use the method we described in this article) and found equal to about 0.1 N *per* supporting leg. This results into a force of 0.3 N for the complete support system, which is equivalent to a force of 0.016 N by actuator. One more time, theses forces are insignificant compared to the one generated by the inertial forces.

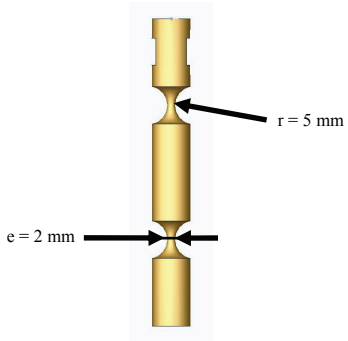

Fig. 11 Support system of the traveling plate

VII. Conclusion

A novel high-resolution and high-speed precision positioning mechanism has been presented, based on a planar parallel quasi-singular flexible architecture, with a decoupled actuating mechanism.

In this paper, we have addressed the modeling of efforts. Two kinds of efforts have been taken into account. The ones generated by the flexible links and those generated by the inertial efforts applied on the micro-stage. These efforts have been modeled and evaluated through simulations for the micro-stage. Hence, it has been possible to make a choice for the actuator and also to design, manufacture and assemble the complete micro-stage. The resolution of positioning for this micro-stage is expected to be around 16 nm with the use of integrated actuator scales which offer a resolution of 0.1 µm.

References

[1] Ronchi S., Company O., Pierrot F., and Fournier A., "PRP Planar Parallel Mechanism in Configurations Improving Displacement Resolution", *in proceedings of the 1st International Conference on Positioning Technologies*, Hamamatsu, Japan, pp.279-284, June 09-11 (2004).

[2] Ronchi S., Company O., Krut S., Pierrot F., and Fournier A., "High Resolution Flexible 3-RRR Planar Parallel Micro-Stage in Near Singular Configuration for Resolution Improvement (Part I)", *in proceedings of the IROS 2005*, Edmonton, Canada (2005).

[3] Howell L. L., *Compliant Mechanisms*, John Wiley & Sons Inc, New York, 459p. (2001).

[4] Henein S., *Conception des Guidages Flexibles*, Presse Polytechniques et Universitaires Romandes, Schüler SA, Lausanne, 225p. (2004).

[5] Chevalier L., and Konieczska S., "Liaisons Elastiques : Calculs et Applications", ENS Cachan, 21p.

[6] Harai T., Herve J. M., and Tanikawa T., "Development of 3 DOF Micro Finger", *in Proceedings of IROS : Intelligent Robots and Systems 96*, Osaka, Japan, Vol. 2, pp.981-987, November 5-8 (1996).

[7] Chung G. B., Yi B.-J., Suh I. K., Kim W. K., and Chung W. K., "Design and Analysis of a Spatial 3-DOF Micromanipulator for Tele-Operation", *in Proceedings of the 2001 IEEE/RSJ International Conference on Intelligent Robots and Systems*, Maui, Hawaii, USA, pp.337-342, October 29 - November 03 (2001).

[8] Hesselbach J., Raatz A., and Kunzmann H., "Perdormance of Pseudo-Elastic Flexure Hinges in Parallel Robots for Micro-Assembly Tasks", *in Proceedings of the CIRP*, pp.329-332, (2004).

[9] Yi B.-J., Chung G. B., Na H. Y., Kim W. H., and Suh I. H., "Design and Experiment of a 3-DOF Parallel Micromechanism Utilizing Flexure hinges", *in Proceedings of IEEE Transactions on Robotics and Automation*, Las Vegas, Nevada, pp.604-612, August (2003).

[10] Ranganath R., Nair P. S., Mruthyunjaya T. S., and Ghosal A., "A Force-Torque Sensor Based on a Stewart Platform in a Near Singular Configuration", *Journal of Mechanism and Machine theory*, Vol. 39, pp.971-998, April 10 (2004).

[11] Clavel R., "Robots Parallèles", *Techniques de l'Ingénieur*, (1994).

[12] Zlatonov D., Fenton R. G., and Benhabib B., "Identification and Classification of the Singular Configurations of Mechanisms", *Mechanism and Machine Theory*, Vol. 33, (6), pp. 743-760, August (1998).

[13] Pernette E., "Robot de Haute Précision à 6 Degrés de Liberté pour l'Assemblage des Microsystèmes", Département de Microtechnique, Ecole Polytechnique Fédérale de Lausanne, Lausanne, 167p. (1998).

[14] Merlet J.-P., Les Robots Parallèles, Hermes, Paris, 304p. (1997).

[15] Williams R. L., "Inverse Kinematics for Planar Parallel Manipulators", *in Proceedings of ASME Design Technical Conferences*, Sacramento, California, 6p., September 14-17 (1997).

[16] Merlet J.-P., "Direct Kinematics of Planar Parallel Manipulators", *in Proceedings of International Conference on Robotics and Automation*, Mineapolis, Minesota, pp.3744-3749, April (1996).